Available online at www.sciencedirect.com
ScienceDirect
European Journal of Mechanics B/Fluids 25 (2006) 602–620

Melnikov analysis and inverse spectral analysis of rogue waves in deep water

C.M. Schober

Department of Mathematics, University of Central Florida, Orlando, FL 32816, USA

Received 6 November 2005; received in revised form 19 February 2006; accepted 20 February 2006

Available online 5 June 2006

Abstract

Rogue waves in deep water are investigated in the framework of the nonlinear Schrödinger (NLS) and the modified Dysthe (MD) equations. We observe that a chaotic regime increases the likelihood of rogue wave formation and that enhanced focusing occurs due to chaotic evolution of the phases. A Melnikov analysis indicates persistence of a homoclinic solution in the MD system which is $\mathcal{O}(\epsilon)$-close to an optimally phase modulated solution of the NLS. The correlation of the Melnikov analysis and the numerical experiments indicates that one approach to predicting rogue waves in realistic oceanic states is to determine the proximity of a sea state to homoclinic data of the NLS. Using the inverse spectral theory of the NLS equation, we show that the development of extreme waves in random oceanic sea states characterized by JONSWAP power spectra is well predicted by the proximity to homoclinic data of the NLS.

PACS: 92.10.Hm; 47.20.Ky; 47.35+i

Keywords: Rogue waves; Freak waves; Homoclinic orbits; Nonlinear Schrödinger equation; Nonlinear focusing; Modulational instability

1. Introduction

Rogue waves are anomalous large amplitude waves which can be very destructive due to the high concentration of wave energy. The formal definition of a rogue wave is a high amplitude wave whose height exceeds 2.2 times the significant wave height H_s of the background sea. In recent years there has been significant interest in understanding the physical processes responsible for the generation of rogue waves and the conditions for which they are most likely to occur. Rogue waves have been observed in both shallow and deep water, with or without the presence of strong currents. Several mechanisms are known that produce large amplitude waves from relatively small ones by focusing the energy. Depending on the specific physical conditions they are: (i) focusing by current refraction [1], (ii) focusing in time and space [2] and (iii) nonlinear focusing [3,4]. A broad overview of these mechanisms is provided in the article [2] and in the monograph [5].

In this paper we investigate the development of rogue waves in deep water due to the Benjamin–Feir (BF) instability and nonlinear focusing. The BF instability is a modulational instability in which a uniform train of surface

E-mail address: cschober@mail.ucf.edu; Tel.: +407 823 0147; fax: +407 823 6253.

0997-7546/$ – see front matter
doi:10.1016/j.euromechflu.2006.02.005

gravity waves is unstable to a weak amplitude modulation. In [3], Henderson et al. examined extreme wave events by simulating the evolution of a periodically perturbed uniform wave train. Due to the BF instability the wave train breaks into periodic groups. Further focusing occurs within each group producing a very large wave with a crest height approximately three times the initial amplitude of the wave train. Since the BF instability is described to leading order by the nonlinear Schrödinger (NLS) equation, they noted that the features of the simulated large waves are consistent with a breather solution of the NLS equation [3].

The NLS equation is the leading order equation in a hierarchy of envelope equations and is derived from the full water wave equations by making a small amplitude, slowly modulated wave approximation with an additional assumption of an $\mathcal{O}(\epsilon)$ narrow banded spectrum [6,7]. Although restrictive, these assumptions are not physically unrealistic. On January 1st 1995 a rogue wave, referred to as the "New Year wave", was measured under the Draupner platform in the North Sea. The maximum wave height of 25.6 m was more than twice the significant wave height of about 10.8 m. The salient point is that an analysis of the ocean state around the New Year wave shows that the envelope of the wave train as a whole is slowly modulated, weakly nonlinear and has a relatively small bandwidth [4]. This supports using the NLS equation and it's higher order extensions as simple mathematical models for the description of rogue waves.

The $\mathcal{O}(\epsilon)$ bandwidth constraint limits the applicability of the NLS equation in 2D as it results in energy leakage to high wave number modes. A more accurate description of water wave dynamics is provided by, for example, the fourth-order modified Dysthe (MD) equation, derived by assuming the bandwidth is $\mathcal{O}(\sqrt{\epsilon})$ and by retaining higher order terms in the asymptotic expansion for the surface wave displacement [8]. The MD equation is able to capture higher order physical effects such as asymmetric evolution of wave packets and side bands and also controls the size of the instability region by limiting the energy leakage to higher modes that is obtained with the 2D NLS equation [8,9].

Based on the insightful observation by Henderson et al. (and separately by Osborne et al. [10]), that simple analytical solutions of the NLS equation such as the breather exhibit many of the properties of rogue waves, we asked the following questions: (i) Are there other solutions of the NLS equation that provide more striking candidates for rogue waves? (ii) The evolution of deep water gravity waves is described only to leading order by the NLS equation. When using more accurate theoretical models, e.g. the MD equation, what are the effects of the higher order terms on the wave dynamics and on the likelihood of rogue wave formation? (iii) Is it possible to develop a diagnostic, such as the "proximity" to homoclinic data for the NLS equation, which will indicate the occurrence of rogue waves for more realistic oceanic sea states, e.g. in random oceanic sea states characterized by the Joint North Sea Wave Project (JONSWAP) power spectra?

We adopt an approach based on the NLS equation, as well as it's higher order generalizations, to study rogue wave dynamics in deep water. In Section 2 elements of the inverse spectral theory of the NLS equation are presented. The Floquet spectral theory is used for constructing analytical solutions of the NLS, for determining the characteristics of the evolution of the wave train, and for interpreting a nonlinear mode decomposition of data.

A linearized analysis of the NLS equation shows that low frequency modes may become unstable and that the number of unstable modes increases with the amplitude of the carrier wave. The complete integrability of the NLS equation allows one to use Bäcklund transformations to compute homoclinic solutions and thus study the nonlinear evolution of the instability [11]. In Section 3 we consider homoclinic orbits of the Stokes wave (or plane wave) for the NLS equation and discuss their interpretation as rogue waves. We consider the more general case when two or more unstable modes are present (see Eq. (8)) and examine the effect of phase modulating the initial wave train on the formation of rogue waves. Since these solutions have a more complex space–time structure, we find they can be "optimally" phase modulated so that the modes are excited simultaneously (also referred to as "nonlinear chirping"), leading to a significant amplification beyond what is predicted by the usual BF modulation instability [12] (see Fig. 3(b)). Phase-modulated wave trains and focusing of nonlinear wave groups in deep water was also examined by Kharif et al. [13].

Phase modulation or the preselection of phases corresponds to a very special situation and it is reasonable to investigate how such a spontaneous alignment of the phases might occur. In Section 4 we examine the effect of homoclinic chaos on the formation of rogue waves. "Noisy" rogue waves, i.e. rogue waves with a chaotic background, are observed in numerical simulations of both the full modified Dysthe (MD) equation and under the restriction to spatially symmetric wave trains. In a chaotic regime of homoclinic type, the solution can evolve close to an optimal phase modulated homoclinic solution for a rather general class of initial conditions, even when the initial data has not

been preselected or phase modulated. We find that chaotic evolution of the phases allows for enhanced focusing to occur [12].

In Section 5 we support the numerical study of the MD equation with a Melnikov analysis which indicates persistence of a homoclinic solution in the MD system in the even regime. Significantly, the Melnikov analysis predicts the same distinguishing spatial features of the perturbed dynamics as those observed in the numerical experiments [12]. The homoclinic orbit (or rogue wave) selected by the Melnikov analysis is $\mathcal{O}(\epsilon)$-close to the optimal phase modulated NLS homoclinic solution (Fig. 3(b)) and is observed in the numerical simulations (Fig. 5(a)). This persistence result substantiates the notion that homoclinic solutions of the NLS equation are significant in modeling rogue waves and led us to conjecture that one approach to predicting rogue waves in realistic oceanic states would be to determine the proximity of a sea state to homoclinic data of the NLS equation.

Developing sea states are described by the JONSWAP power spectrum (e.g., [14]). In Section 6 we investigate the formation of rogue waves in random oceanic sea states characterized by the JONSWAP power spectra [15]. We clarify the dependence of rogue wave events on the phases in the "random phase" reconstruction of the surface elevation (see Eq. (22)). We find that the phase information is as important as the amplitude and peakedness of the wave when determining the occurrence of rogue waves. Random oceanic sea states characterized by JONSWAP data are not small perturbations of Stokes wave solutions. As a consequence, it is difficult to investigate the generation of rogue waves in more realistic sea states using a linear stability analysis (as in the Benjamin–Feir instability).

Our approach uses the inverse spectral theory of the NLS equation to examine a nonlinear mode decomposition of JONSWAP type initial data. We introduce a spectral quantity, the "splitting distance" δ between simple points in the discrete Floquet spectrum of the associated AKNS problem, and use it to determine the proximity in spectral space to instabilities of solutions of the NLS equation and homoclinic orbits. Our main results in this section are: (1) JONSWAP data can be quite near data for homoclinic orbits of complicated N-phase solutions. For fixed values of α and γ in the JONSWAP spectrum, as the phases in the initial data are randomly varied, the proximity δ to homoclinic data varies. (2) The results of several hundred simulations, where the parameters and phases in the JONSWAP initial data are varied, indicate that rogue waves develop whenever the splitting distance is small, and do not when the splitting distance is large [15]. These results are shown to be applicable to the MD equation as well. Concluding remarks are provided in Section 7.

2. Integrable structure of the NLS equation

One of the simplest nonlinear models for describing the propagation of unidirectional surface waves on deep water is the nonlinear Schrödinger (NLS) equation,

$$Nu \equiv \mathrm{i}u_t + u_{xx} + 2|u|^2 u = 0, \tag{1}$$

which can be written in Hamiltonian form

$$\mathrm{i}\partial_t \begin{pmatrix} u \\ u* \end{pmatrix} = J \begin{pmatrix} \delta H/\delta u \\ \delta H/\delta u* \end{pmatrix}, \quad \text{with } J = \begin{pmatrix} 0 & 1 \\ -1 & 0 \end{pmatrix} \tag{2}$$

and Hamiltonian

$$H(u, u*) = \int_0^L \left(|u_x|^2 - |u|^4\right) \mathrm{d}x. \tag{3}$$

The complete integrability of the NLS equation is established using the associated linear systems (the so-called Lax pair)

$$\mathcal{L}^{(x)}\phi = \begin{pmatrix} D + \mathrm{i}\lambda & -u \\ u^* & D - \mathrm{i}\lambda \end{pmatrix} \begin{pmatrix} \phi_1 \\ \phi_2 \end{pmatrix} = 0, \quad \mathcal{L}^{(t)}\phi = 0, \tag{4}$$

where D denotes the derivative with respect to x, λ is the spectral parameter and ϕ is the eigenfunction [6]. These systems have a common nontrivial solution $\phi(x, t; \lambda)$, provided the potential $u(x, t)$ satisfies the NLS equation. $\mathcal{L}^{(t)}$ is not specified explicitly as it is not used in our subsequent analysis.

For periodic boundary conditions, $u(x + L, t) = u(x, t)$, one can characterize u (for any fixed time t) in terms of its Floquet spectrum $\sigma(u) = \{\lambda \in \mathbb{C} \mid \mathcal{L}^{(x)}\phi = 0, |\phi| \text{ bounded } \forall x\}$. The Floquet spectrum can be expressed in terms

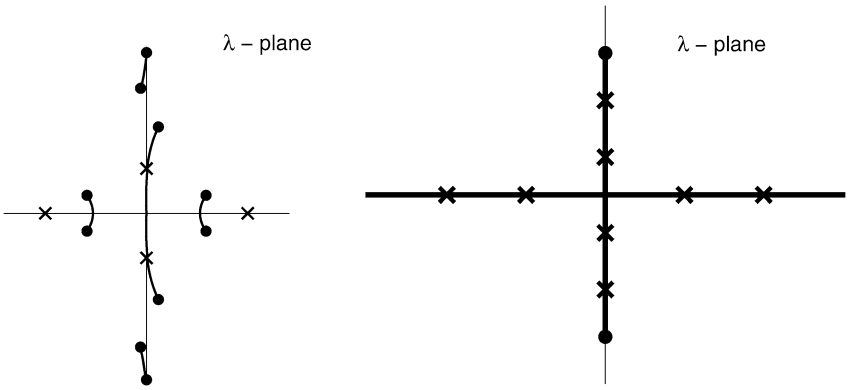

Fig. 1. Spectrum of an unstable N-phase solution (left) and a plane wave solution (right).

of the transfer matrix $M(x+L;u,\lambda)$ across a period, where $M(x;u,\lambda)$ is a fundamental solution matrix of the Lax pair (4). Introducing the Floquet discriminant $\Delta(u,\lambda)=\mathrm{Trace}[M(x+L;u,\lambda)]$, one obtains [7]

$$\sigma(u)=\left\{\lambda\in\mathbb{C}\mid \Delta(u,\lambda)\in\mathbb{R},\ -2\leqslant\Delta(u,\lambda)\leqslant 2\right\}. \tag{5}$$

The distinguished points of the periodic/antiperiodic spectrum, where $\Delta(\lambda,u)=\pm 2$, are: (a) simple points $\{\lambda_j^s \mid \mathrm{d}\Delta/\mathrm{d}\lambda\neq 0\}$ and (b) double points $\{\lambda_j^d \mid \mathrm{d}\Delta/\mathrm{d}\lambda=0, \mathrm{d}^2\Delta/\mathrm{d}\lambda^2\neq 0\}$. The Floquet discriminant functional $\Delta(u,\lambda)$ is invariant under the NLS flow and encodes the infinite family of constants of motion of the NLS (parametrized by the λ_j^s).

The Floquet spectrum (5) of a generic NLS potential consists of the entire real axis plus additional curves (called bands) of continuous spectrum which terminate at the simple points λ_j^s. N-phase solutions are those with a finite number of bands of continuous spectrum. Double points arise when two simple points have coalesced and their location is important.

The nonlinear mode content of a solution of the NLS equation can be determined using the direct spectral transform. The spatial structure and dynamical stability of these modes is determined by the order and location of the corresponding λ_j as follows: (a) Simple points correspond to stable active degrees of freedom. (b) Double points label all additional potentially active degrees of freedom. Real double points correspond to stable inactive (zero amplitude) modes. Complex double points are associated with all the unstable active modes and label the corresponding homoclinic orbits [16,17].

Fig. 1 shows the spectrum of a typical unstable N-phase solution. The simple periodic eigenvalues and the double points are denoted by circles and crosses, respectively. In this case there are N bands of spectrum determined by the $2N$ simple points λ_j^s and $2M$ embedded complex double points λ_j^d. The spectrum for a nearby semi-stable N-phase solution, where the complex double points are split $\mathcal{O}(\epsilon)$, is given in Fig. 8(a) (which shows only the spectrum in the upper half plane).

As an example, the Floquet discriminant of a plane wave solution $u(x,t)=a\,\mathrm{e}^{2\mathrm{i}a^2t}$ is readily computed to be $\Delta(a,\lambda)=2\cos(\sqrt{a^2+\lambda^2}L)$. Then, the associated Floquet spectrum consists of the continuous bands $\mathbb{R}\cup[-\mathrm{i}a,\mathrm{i}a]$, and a discrete part containing the simple periodic/antiperiodic eigenvalues $\pm\mathrm{i}a$, and the infinite sequence of double points (see Fig. 1)

$$\lambda_j^2=(j\pi/L)^2-a^2,\quad j\in\mathbb{Z}. \tag{6}$$

Of these, if $[aL/\pi]=M$ (where $[p]=$ largest integer $\leqslant p$, $p>0$), $2M$ are complex (pure imaginary) double points, while the remaining λ_n's for $|n|>M$ are real.

The N-phase quasiperiodic solutions of the NLS equation have the form [18–20],

$$u(x,t)=u_0\,\mathrm{e}^{\mathrm{i}(k_0x-\omega_0t)}\frac{\Theta(\boldsymbol{W}^-|\tau)}{\Theta(\boldsymbol{W}^+|\tau)}, \tag{7}$$

where Θ is the Riemann theta function, $\boldsymbol{W}^\pm=(W_1^\pm,\ldots,W_N^\pm)$, and the phases evolve according to $W_j^\pm=(\kappa_jx+\Omega_jt+\theta_j^\pm)$. The external phase as well as the wavenumbers κ_j and frequencies Ω_j are expressible in terms of

algebraic-geometric data including the branch points of the associated Riemann surface (namely, the simple points λ_j^s of the Floquet spectrum), Abelian integrals of certain meromorphic differentials and the Abel map. The invariance of the spectrum implies κ_j and Ω_j are constants. For a generic N-phase solution, the isospectral set comprises an N-dimensional torus characterized by the phases $W_j^{\pm}$. If the spectrum contains complex double points, then the N-phase solution may be unstable. The instabilities correspond to orbits homoclinic to the N-phase torus.

3. Homoclinic solutions of the NLS equation as rogue waves

An important physical prediction of the NLS equation is the modulational or Benjamin–Feir instability for periodic potentials. Modulationally unstable periodic solutions have homoclinic orbits which can be used to model rogue waves. An example of this is provided by the plane wave solution, $u_0(x,t) = a\,\mathrm{e}^{2\mathrm{i}|a|^2 t}$, which has M linearly unstable modes (UMs) with growth rates $\sigma_n^2 = \mu_n^2(\mu_n^2 - 4a^2)$, $\mu_n = 2\pi n/L$, provided

$$0 < (\pi n/L)^2 < |a|^2 \tag{8}$$

is satisfied (the number M of UMs is the largest integer satisfying $0 < M < |a|L/\pi$). That is, the plane wave is unstable with respect to long wavelength perturbations. The condition for the solution to be linearly unstable is the same as the condition for complex double points in the spectrum. For each UM there is a corresponding homoclinic orbit; moreover, "combination" homoclinic orbits associated with two or more UMs can be constructed.

Linearizing to study stability provides information about the instability only for short times, for as long as the linearization is approximately correct. Global representations of the homoclinic orbits can be obtained by exponentiating the linear instabilities via Bäcklund transformations [21,22]. A single homoclinic orbit of the plane wave is given by

$$u(x,t) = a\,\mathrm{e}^{-2\mathrm{i}a^2 t}\left(\frac{1 + 2\cos(px)\,\mathrm{e}^{\sigma_1 t + 2\mathrm{i}\phi + \gamma} + A_{12}\,\mathrm{e}^{2\sigma_1 t + 4\mathrm{i}\phi + 2\gamma}}{1 + 2\cos(px)\,\mathrm{e}^{\sigma_1 t + \gamma} + A_{12}\,\mathrm{e}^{2\sigma_1 t + 2\gamma}}\right) \tag{9}$$

where $A_{12} = 1/\cos^2\phi$, $\sigma_1 = \pm p\sqrt{4a^2 - p^2}$, $\phi = \sin^{-1}(p/2a)$, and $p = \mu_n = 2\pi n/L$, satisfies (8) for some integer n. Each UM has an associated homoclinic orbit characterized by the mode $p = \mu_n$.

Fig. 2 shows the space–time plot of the amplitude $|u(x,t)|$ of a homoclinic orbit ($a = 0.5$, $L = 2\sqrt{2}$ and $p = 2\pi/L$) with one UM. This homoclinic solution represents the simplest prototype of rogue wave. As $t \to \pm\infty$, solution (9) limits asymptotically to the plane wave; i.e. the plane wave behavior dominates the motion for most of its lifetime. As $t \to t_0$ ($t_0 \approx 16$), nonlinear focusing occurs due to the BF instability and the solution rises to a maximum height $2.4a$.

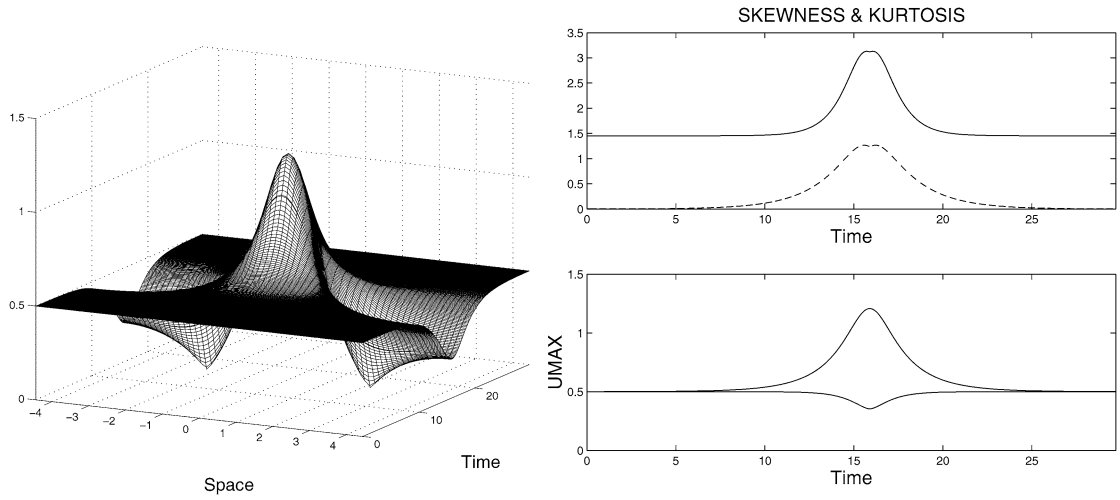

Fig. 2. Rogue wave solution of the NLS equation corresponding to one unstable mode.

An almost equally dramatic wave trough occurs close to the crest of the rogue wave as a result of wave compression due to wave dislocation. The amplitude amplification factor is given by

$$f = \frac{|u_{\max}|}{\lim_{t\to\pm\infty}|u(x,t)|} \approx 2.4. \tag{10}$$

In general, f depends upon the wavenumber of the modulation. As the wave number decreases, the amplification factor increases reaching the following limit

$$f_{\max} = \lim_{\kappa\to 0} f(\kappa) = 3, \tag{11}$$

although the waves take longer to reach their maximum height since their growth rate is smaller [23].

In this paper, accompanying the surface plots are: (i) the corresponding skewness (dashed line) and kurtosis (solid line) as functions of time as well as (ii) the maximum of the amplitude (UMAX) and the mean of the wavefield as functions of time. The skewness and kurtosis are the third and fourth statistical moments of the wavefield respectively (see Appendix A for an interpretation in terms of rogue wave events). At $t \approx 10$ the kurtosis starts to increase indicating the onset of the BF instability and at $t \approx 16$ it reaches it's maximum. However the kurtosis barely exceeds three and as a result this is not as interesting a case from the perspective of rogue waves as the following examples.

3.1. Phase modulated rogue waves

As the number of UMs increases, the space–time structure of the homoclinic solutions becomes more complex. We find that when two or more UMs are present the initial wave train can be phase modulated to produce additional focusing. The family of homoclinic orbits (i.e. rogue waves) associated with two UMs is given by [24,12]

$$u(x,t) = a\,\mathrm{e}^{2\mathrm{i}a^2 t}\,\frac{g(x,t)}{f(x,t)}, \tag{12}$$

where

$$\begin{aligned}
f(x,t) &= 1 + 2\cos(p_1 x)\,\mathrm{e}^{\sigma_1 t} + A_{12}\,\mathrm{e}^{2\sigma_1 t} + 2\cos(p_3 x)\,\mathrm{e}^{\sigma_3 t+\gamma} + A_{34}\,\mathrm{e}^{2(\sigma_3 t+\gamma)} \\
&\quad + 2\big[A_{13}\cos(p_1+p_3)x + A_{23}\cos(p_3-p_1)x\big]\,\mathrm{e}^{(\sigma_1+\sigma_3)t+\gamma} + 2A_{12}A_{13}A_{23}\cos(p_3 x)\,\mathrm{e}^{(2\sigma_1+\sigma_3)t+\gamma} \\
&\quad + A_{12}A_{13}^2A_{23}^2A_{34}\,\mathrm{e}^{2(\sigma_1+\sigma_3)t+2\gamma} + 2A_{13}A_{23}A_{34}\cos(p_1 x)\,\mathrm{e}^{(\sigma_1+2\sigma_3)t+2\gamma}, \\
g(x,t) &= 1 + 2\,\mathrm{e}^{2\mathrm{i}\phi_1}\cos(p_1 x)\,\mathrm{e}^{\sigma_1 t} + A_{12}\,\mathrm{e}^{4\mathrm{i}\phi_1}\,\mathrm{e}^{2\sigma_1 t} + 2\,\mathrm{e}^{2\mathrm{i}\phi_3}\cos(p_3 x)\,\mathrm{e}^{\sigma_3 t+\gamma} \\
&\quad + A_{34}\,\mathrm{e}^{4\mathrm{i}\phi_3}\,\mathrm{e}^{2(\sigma_3 t+\gamma)} + A_{12}A_{13}^2A_{23}^2A_{34}\,\mathrm{e}^{4\mathrm{i}(\phi_1+\phi_3)}\,\mathrm{e}^{2(\sigma_1+\sigma_3)t+2\gamma} \\
&\quad + 2A_{13}A_{23}A_{34}\,\mathrm{e}^{2\mathrm{i}(\phi_1+2\phi_3)}\cos(p_1 x)\,\mathrm{e}^{(\sigma_1+2\sigma_3)t+2\gamma} + 2A_{12}A_{13}A_{23}\,\mathrm{e}^{2\mathrm{i}(2\phi_1+\phi_3)}\cos(p_3 x)\,\mathrm{e}^{(2\sigma_1+\sigma_3)t+\gamma} \\
&\quad + 2\,\mathrm{e}^{2\mathrm{i}(\phi_1+\phi_3)}\big[A_{13}\cos(p_1+p_3)x + A_{23}\cos(p_3-p_1)x\big]\,\mathrm{e}^{(\sigma_1+\sigma_3)t+\gamma}, \\
A_{jk} &= \left(\frac{\sin\frac{1}{2}(\phi_j-\phi_k)}{\sin\frac{1}{2}(\phi_j+\phi_k)}\right)^2, \qquad \sigma_j = \pm\mu_j\sqrt{4a^2-\mu_j^2}.
\end{aligned}$$

As in the last example, provided $p_1 = \mu_n$ and $p_3 = \mu_m$ satisfy (8), the solution decays to the plane wave solution, as $t \to \pm\infty$, and the rogue wave lies hidden beneath the background plane wave for most of its lifetime. This rogue wave is characterized by the two modes $\cos(p_1 x)$ and $\cos(p_3 x)$, whose temporal separation is determined by the parameter γ. Figs. 3(a)–(b) illustrate the combination homoclinic orbit (12) obtained when $a = 0.5$, $L = 4\sqrt{2}$, $p_3 = 2p_1 = 2\pi/L$ and $\phi_j = \sin^{-1}(\mu_j/2a)$, for $\gamma = 0.1$ and $\gamma = 0.2$, respectively. In Fig. 3(a) the modes are well separated and the maximum value of the amplitude is roughly three times the plane wave amplitude (its maximum is 1.4). In this example the kurtosis is well above three.

Both the temporal separation of the two modes and the maximum amplitude that can be achieved depend upon the parameter γ. A homoclinic orbit of maximum amplitude is obtained when the two UMs are excited simultaneously. This is an example of "optimal" phase modulation or "nonlinear chirping", where the phases in the initial data have been selected so that the solution chirps up to a maximum height. In Fig. 3(b) the rogue wave rises to a height of approximately 4.1 times the height of the background carrier wave (the maximum height is 2.1). The kurtosis is also significantly larger, $m_4 \approx 14$. We note that Fig. 3(a) shows focusing due to only a weak amplitude modulation of the

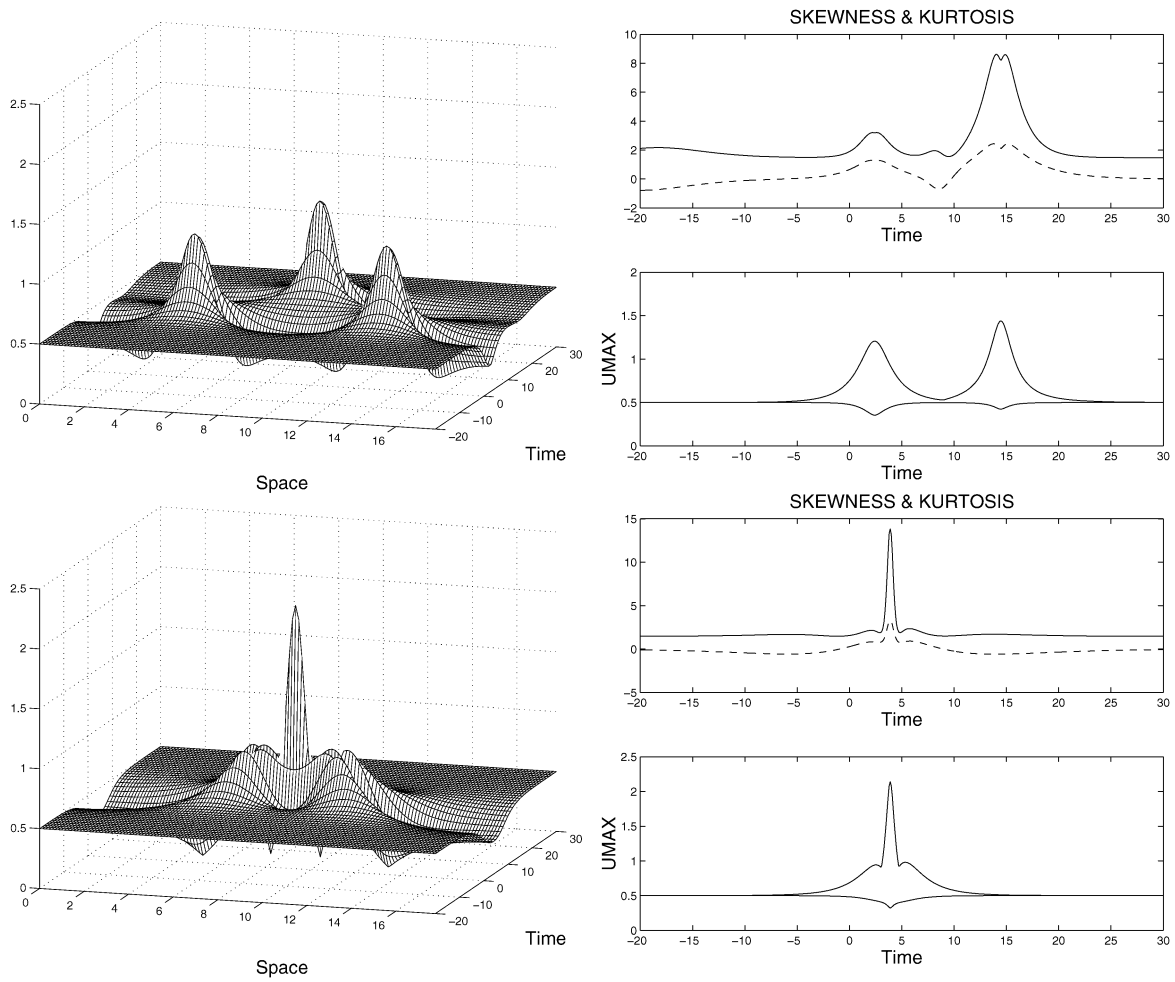

Fig. 3. Rogue wave solutions of the NLS corresponding to two unstable modes without phase modulation (top) and with phase modulation (bottom).

initial wave train. The growth in UMAX starting at $t \approx -5$ and at $t \approx 10$ is due to the BF instability. However, in Fig. 3(b) focusing due to both an amplitude and a phase modulation occurs. The growth in UMAX visible at $t \approx -5$ is due to the BF instability while the additional very rapid focusing at $t \approx 3.4$ is due to the phase modulation.

In general it is possible to choose the phases in the homoclinic orbits (general formulas can be found in Ref. [12]) so that any number of UMs phase lock. Figs. 4(a) and 4(b) illustrate two members of the family of homoclinic orbits corresponding to three UMs; in Fig. 4(a) the modes are separated and in Fig. 4(b) the modes have coalesced. The rogue wave attains a height of approximately three and six times the height of the background carrier wave, respectively. As before, the striking difference in wave amplification is due to the additional phase modulation. Further generalization can be achieved using a linearly unstable quasi-periodic (in time) theta function solution of the NLS equation as a carrier wave. Homoclinic orbits for such solutions can also be constructed explicitly, providing an analytical characterization of rogue waves generated from a quasiperiodic background state rather than a plane wave state.

4. Rogue wave solutions of the modified Dysthe equation

In this section we consider a broader bandwidth modified NLS equation introduced by Trulsen and Dysthe [8]. The equation arises as a higher order asymptotic approximation of slowly modulated periodic wave trains in deep water under the assumption that the wave slope ka is $\mathcal{O}(\epsilon)$ (a is the size of the initial surface displacement), while the

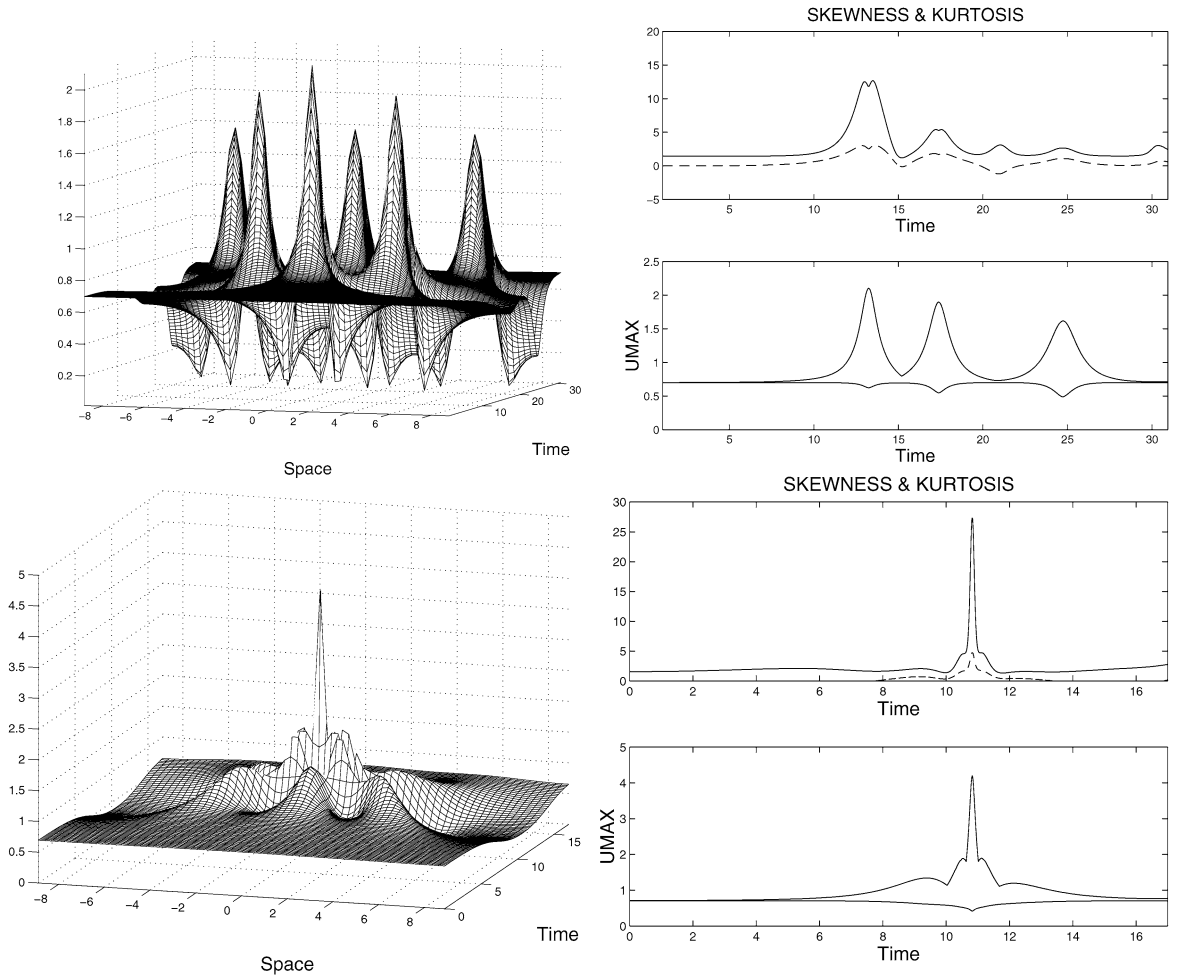

Fig. 4. Rogue waves solutions of the NLS corresponding to three unstable modes without phase modulation (top) and with phase modulation (bottom).

bandwidth $|\Delta k|/k$ and $(kh)^{-1}$ (h is the water depth) are $\mathcal{O}(\epsilon^{1/2})$. In this case one obtains the modified Dysthe (MD) equation

$$Nu + \mathrm{i}\epsilon^{1/2}\left(\frac{1}{2}u_{xxx} - 6|u|^2u_x + u^2u_x^* - 2u\mathrm{i}\big[H\big(|u|^2\big)\big]_x\right) + \epsilon\frac{5}{16}u_{4x} + \mathrm{i}\epsilon^{3/2}\frac{7}{32}u_{5x} = 0, \tag{13}$$

where Nu is the NLS operator defined in (1) and $H(f)$ represents the Hilbert transform of the function f [8]. Our interest lies in determining how the higher order terms effect the wave dynamics and the likelihood of rogue wave formation.

In earlier work we experimentally and theoretically studied the long-time evolution of modulated periodic Stokes waves in deep water. Both laboratory and numerical experiments with a higher order NLS (HONLS) equation, derived under the traditional narrow bandwidth assumption, consistently showed that when $N \geqslant 2$ unstable modes are present, the evolution is temporally chaotic and not reproducible [25,26]. We found that the higher order terms are responsible for driving waves ("left-or-right" moving waves) to evolve chaotically across a fixed state.

The HONLS equation may be viewed as a "near-integrable" equation and, as a result, the dynamics in the chaotic regime can be understood by appealing to the spectral theory of the NLS equation. The spectrum, while invariant for the NLS equation, evolves due to the higher order terms in the HONLS equation. Homoclinic transitions in the spectrum occur when the spectrum evolves between two topologically different configurations. An analysis of the spectral decomposition of the laboratory data and of the HONLS data yielded numerous homoclinic transitions in the

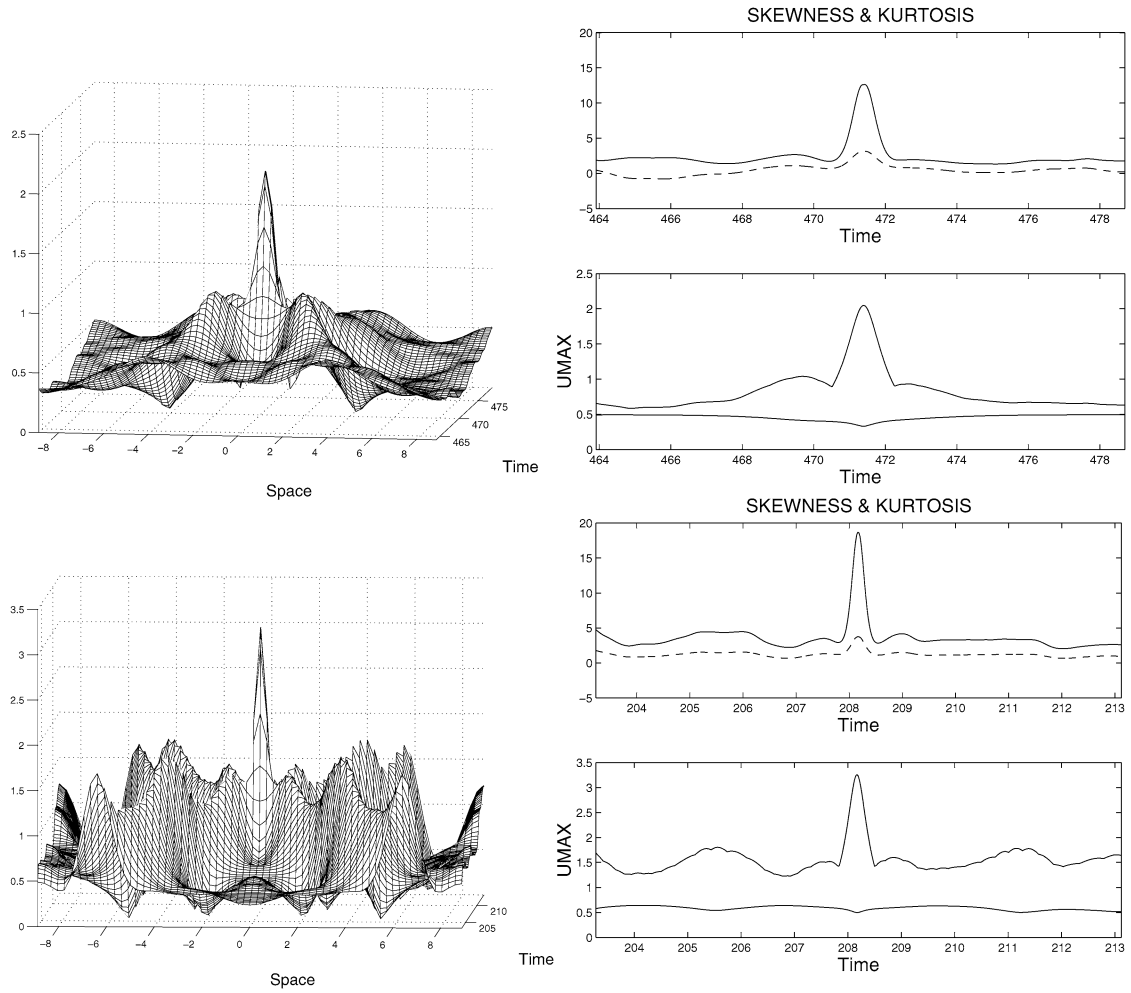

Fig. 5. Rogue waves solutions for the even MD equation when two (top) and three (bottom) unstable modes are present.

spectrum [25]. Fig. 7 shows the spectrum at a sampling of time slices in the chaotic regime where the topological changes are clearly visible. Recalling the construction of a finite phase solution (7) from it's spectral data, where the Riemann surface as well as the phases depend intimately on the discrete eigenvalues λ_j, we find that due to the homoclinic transitions the phases are evolving chaotically [26].

What effect does the chaotic phase evolution have on the generation of rogue waves? Since the HONLS dynamics is chaotic in the presence of $N \geqslant 2$ UMs, we examine the MD dynamics in the two and three UM regime. We begin by considering the restriction to spatially symmetric wave trains $u(-x,t) = u(x,t)$, resulting in the "even" MD equation

$$\mathrm{i}u_t + u_{xx} + 2|u|^2 u = \epsilon u_{xxxx}. \tag{14}$$

Initial data for solutions with two UMs are obtained by linearizing (12) about $t = 0$,

$$u(x,0) = a\big[1 + 4\mathrm{i}\big(\epsilon_1 \sin\phi_1\, \mathrm{e}^{\mathrm{i}\phi_1} \cos p_1 x + \epsilon_3 \sin\phi_3\, \mathrm{e}^{\mathrm{i}\phi_3} \cos p_3 x\big)\big]$$

where the parameter values are given as in (12). Fig. 5(a) illustrates a striking rogue wave solution of Eq. (14) for $\epsilon_1 = 10^{-4}$ and $\epsilon_3 = 10^{-5}$. The solution quickly ($t \approx 31$) develops irregularities and becomes chaotic. At $t \approx 471.2$ a rogue wave rises up from the plane wave state and develops a crest with an amplitude of approximately four times the background wave height. This MD rogue wave structure is close to the maximum amplitude rogue wave of the NLS obtained when $\gamma = 0.2$ (compare Fig. 5(a) with Fig. 3(b)). Numerical experiments in the three UM regime also show that after the solution becomes chaotic rogue waves develop (see Fig. 5(b)). At $t \approx 208$ a rogue wave develops with

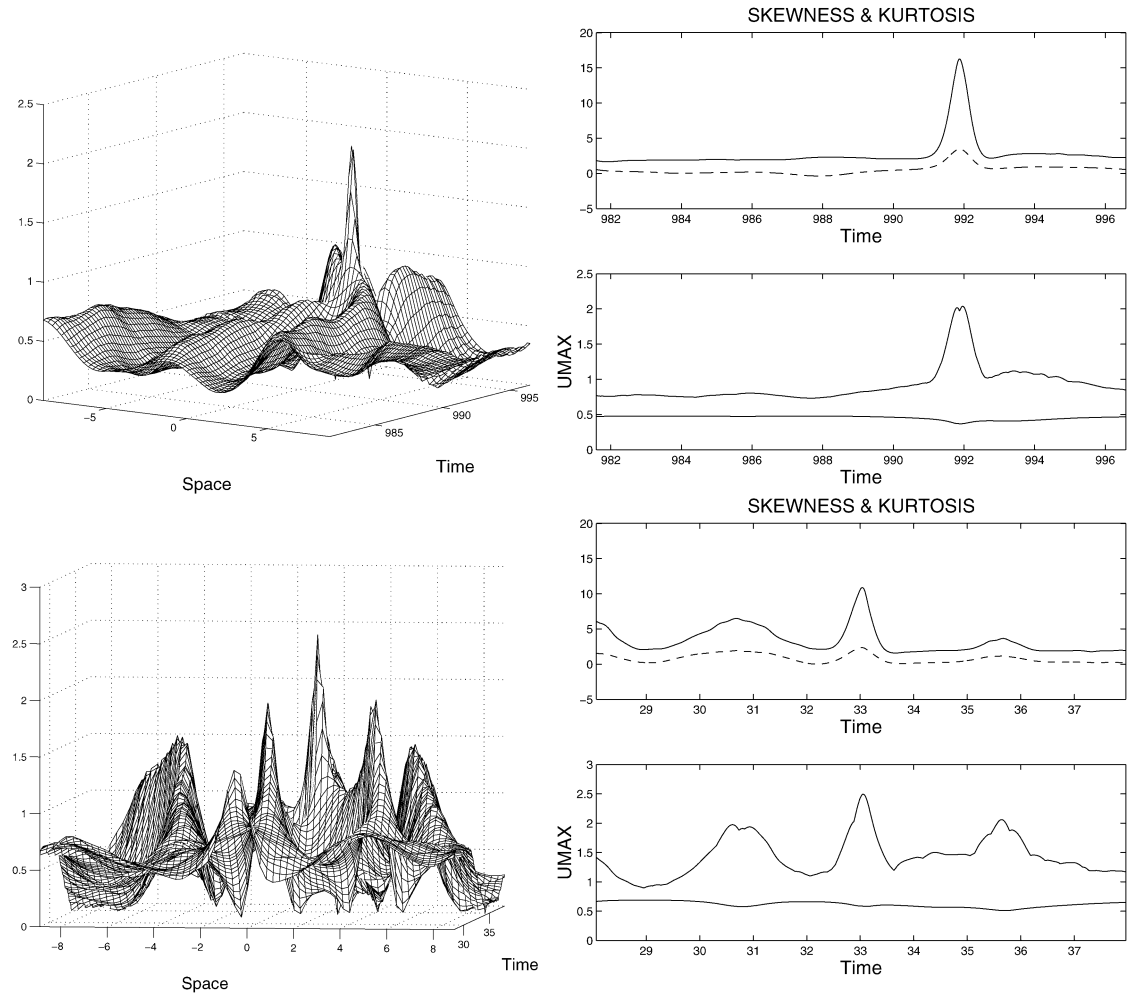

Fig. 6. Rogue wave solutions for the full MD equation when two (top) and three (bottom) unstable modes are present.

a wave amplitude amplification factor of almost five. Similarly, this solution is close to the optimal phase modulated homoclinic solution in the three UM regime.

In experiments using the full MD equation (13) we obtain amplitude amplification factors slightly smaller than in comparable experiments (with the same initial data, parameter values etc.) using the even MD equation. The higher order terms in (13) break the spatial symmetry and prevent a complete spatial coalescence of the nonlinear modes. In Figs. 6(a)–(b) the rogue wave solutions of the full MD (in the two and three UM regime) clearly lose spatial symmetry.

We performed extensive numerical experiments using the MD model in the two and three UM regimes, varying both the perturbation strength ϵ and the values of the parameters in the initial data. The coalesced homoclinic orbit emerges generically for these cases and appears to be a structurally stable feature of the perturbed dynamics. We find that the chaotic regime allows further focusing to occur due to chaotically generated optimal phase modulations. The diagnostics in Section 6, which give the wave strengths obtained in the NLS and MD experiments as a function of the spectral "splitting" distance, substantiate that enhanced focusing occurs for the MD equation. It is readily observed in Fig. 10 that larger amplitude waves (and more of them) are obtained for the MD equation. This suggests that the underlying chaotic dynamics in the MD equation increases the likelihood of rogue waves as compared to predictions by the NLS equation.

The Melnikov analysis in the next section provides necessary conditions for the persistence of a homoclinic solution in the MD system which is $\mathcal{O}(\epsilon)$-close to the NLS coalesced homoclinic solution. These results indicate that the

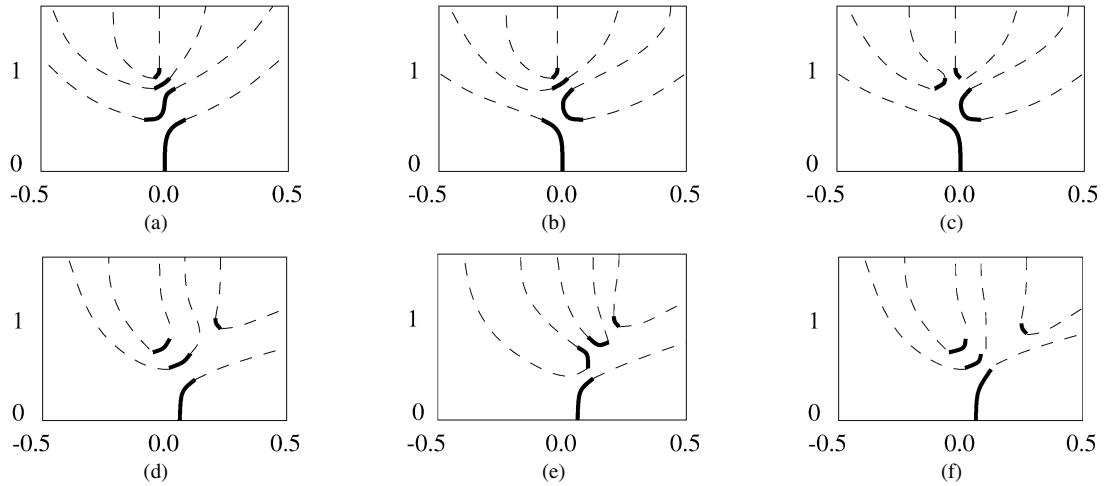

Fig. 7. Spectral plots corresponding to times of (a) 0.0, (b) 0.5, (c) 1.0, (d) 2.0, (e) 2.1, (f) 2.6. Solid darkened curves are curves of spectrum. Curves of real Δ (the dashed curves) have been included to give an indication of the topological changes in the spectrum.

presence of homoclinic orbits in the unperturbed model plays a significant role in both the perturbed chaotic evolution and in the generation of rogue waves in the full MD equation.

5. Melnikov analysis

In this section we discuss our results on the persistence of isolated homoclinic orbits for the MD equation [12]. Melnikov type techniques are used to measure the breakup of homoclinic orbits of the unstable plane wave solution in the MD equation. The Melnikov integrals, set up using phase space information provided by the Floquet discriminant, measure the splitting distance between invariant manifolds. The zeros of the Melnikov integrals provide conditions for transversal intersections of the invariant manifolds, indicating the persistence of homoclinic orbits and the presence of homoclinic chaos. Originally developed for ODEs [27], in recent years Melnikov theory has been generalized to near integrable nonlinear wave equations, usually for the case of even spatial symmetry [28,29,24,30,31]. A Melnikov analysis of noneven chaotic dynamics was introduced for a symmetry-breaking damped-driven perturbation of the NLS equation [32].

5.1. Phase space geometry

The even MD equation (14) can be interpreted as a Hamiltonian system on the Sobolev space $\mathcal{H}_{e,p}$ of even, periodic functions, with Hamiltonian functional

$$H_\epsilon(u,u^*) = \int_0^L \left(|u_x|^2 - |u|^4 - \epsilon|u_{xx}|^2\right) \mathrm{d}x.$$

On the invariant plane $\Pi = \{u(x,t) \mid \partial_x u(x,t) = 0\}$, the dynamics is simply described in terms of a two-parameter family of plane wave solutions $u_a(t;a,\varphi) = a\,\mathrm{e}^{\mathrm{i}(2a^2t+\varphi)}$. The stability type of these solutions is determined by solving Eq. (14) linearized about u_a, using a complex Fourier series expansion of the form $\sum_{j=1}^{\infty} a_j\,\mathrm{e}^{\sigma_j t}\cos jx$.

In the two UM mode regime, for $\epsilon = 0$ and $a_0 < a < a_1$, one obtains growth rates

$$\sigma_j = \pm j\sqrt{a^2 - (\pi j/L)^2}, \quad j = 1,2,$$

corresponding to the two-dimensional stable and unstable eigenspaces of the invariant set $\mathcal{S}_a = \{u_a \mid a_0 < a < a_1\}$, as well as an infinite number of center modes characterized by complex conjugate pairs of eigenvalues $\lambda_j = \pm 2\mathrm{i}\sqrt{(\pi j/L)^2 - a^2}$, $j \geqslant 3$.

As described in Section 3, the invariant set $\mathcal{S}_a$ possesses global two-dimensional stable and unstable manifolds, explicitly parametrized in terms of formula (12) for the two-dimensional family of homoclinic solutions (in expression (12), parameter a and the initial phase of the plane wave solutions are coordinates on $\mathcal{S}_a$, while γ_1 and γ_3 parametrize the individual homoclinic orbits). When $\epsilon \neq 0$, the perturbed dynamics takes place in the codimension two invariant subspace $\mathcal{F} = \{u \in \mathcal{H}_{e,p} \mid H_\epsilon(u, u*) = C_H, I(u, u*) = C_I\}$, where $I = \int_0^L |u|^2 \,\mathrm{d}x$ is the L^2-norm of u, which is preserved by the perturbation. For Eq. (14), two main questions need to be addressed. Persistence of invariant manifolds (the singular perturbation makes the proof delicate, though techniques developed by C. Zeng [33] should guarantee at least that much); and persistence of homoclinic structures, such as homoclinic tubes, which explain the features of the irregular dynamics observed numerically.

Persistence of local invariant manifolds is both expected and supported by the numerical evidence; heuristically, we assume this to determine the number of measurements needed to establish transversal intersections of the invariant manifolds. In the two UM regime, the codimension two locally invariant center-stable and center-unstable manifolds $\mathcal{W}_\epsilon^{\mathrm{cs,cu}}(\mathcal{S}_a)$ will intersect transversally along a codimension four locally invariant submanifold $\mathcal{W}_\epsilon^{\mathrm{cs}} \cap \mathcal{W}_\epsilon^{\mathrm{cu}}$. Since splitting does not occur in the directions normal to the invariant subspace $\mathcal{F}$, it is sufficient to measure the splitting distance between the persistent invariant manifolds along a two-dimensional vector transversal to $\mathcal{W}_0^{\mathrm{cs}} \cap \mathcal{W}_0^{\mathrm{cu}}$. In order to define suitable measurements, some results about the integrable structure of the unperturbed NLS equation are needed.

5.2. Fundamental invariants

The Floquet discriminant functional is invariant under the NLS evolution, and thus encodes the infinite family of constants of motion (in fact, parametrized by $\lambda \in \mathbb{C}$). We briefly describe the results of Y. Li and D.W. McLaughlin [34], which show how the critical structure of the Floquet discriminant (as a functional on $\mathcal{H}_{e,p}$) is in one-to-one correspondence with critical level sets of solutions of the unperturbed PDE.

Given a solution u_c with a purely imaginary critical point λ^c, regarding λ^c as a functional on a neighborhood $\mathcal{U}$ of u_c, one has

$$\frac{\partial}{\partial\lambda}\Delta(\lambda; u)\bigg|_{\lambda^c(u)} = 0; \qquad \lambda^c(u_c) = \lambda^c.$$

The following invariant functional $\boldsymbol{F} : \mathcal{U} \to \mathbb{R}$, $\boldsymbol{F} := \Delta(\lambda^c(u); u)$ is locally smooth, provided $\frac{\mathrm{d}^2}{\mathrm{d}\lambda^2}\Delta(\lambda, u) \neq 0, \forall u \in \mathcal{U}$. Then, the sequence $F_j(u) = \Delta(\lambda_j^c(u), u)$, generated as λ_j^c varies among the critical points of the potential u, defines a natural sequence of constants of motion in the following sense. First, it provides a Morse-function type approach to the description of the topology of level sets of solutions of the integrable PDE (i.e., the stratification is described by identifying the critical level sets, labeled by the double points of the associated Floquet spectrum). Second, the sequence $\{F_j\}_{j=1}^\infty$ provides a local description of the strata which are close to critical level sets of saddle type (this is important when considering the effects of perturbations).

The local analysis is encoded in the first and second variation of the $F_j's$. The gradient of F_j has the following explicit representation [34]; if $\vec{\psi}^\pm(x, \lambda)$ are the Bloch eigenfunctions (common eigenfunctions of the Lax operator $\mathcal{L}^{(x)}$ at (u, λ) and the shift operator $(\mathcal{S}\psi)(x) = \psi(x + L)$), then

$$\frac{\delta F_j}{\delta\vec{u}}(u) = \mathrm{i}\frac{\sqrt{\Delta^2 - 4}}{W[\psi^+, \psi^-]}\begin{bmatrix} \psi_2^+\psi_2^- \\ -\psi_1^+\psi_1^- \end{bmatrix}\bigg|_{\lambda=\lambda^c}. \tag{15}$$

We observe that $\delta F_j/\delta\vec{u}(u_c) = 0$, that is the functional is critical at the critical level set. On the other hand, if u^H is the homoclinic orbit in the isospectral level set of u_c, then

$$\frac{\delta F_j}{\delta\vec{u}}\big(u^H\big) = \mathrm{i}\frac{\sqrt{\Delta^2 - 4}}{W[\Psi^+, \Psi^-]}\begin{bmatrix} \Psi_2^+\Psi_2^- \\ -\Psi_1^+\Psi_1^- \end{bmatrix}\bigg|_{\lambda=\lambda^d} \tag{16}$$

does not vanish. Therefore $\delta F_j/\delta\vec{u}(u^H)$, $j = 1, \ldots, M$ (M being the number of complex double points) define directions transversal to the homoclinic manifold and can be used to construct Melnikov-type measurements.

5.3. The Melnikov integrals

In this section we generalize the formulas for the Melnikov integrals obtained in [34] to the case of 2 complex double points (ν_1, ν_2) and compute them for the conservative perturbation (14).

Denoting with $f(\vec{u}) = (u_{xxxx}, u^*_{xxxx})^{\mathrm{T}}$ the vector of the perturbation, the components of the distance vector between the persistent invariant manifolds $W^{\mathrm{cs}}_{\epsilon}(\mathcal{S}_a)$ and $W^{\mathrm{cu}}_{\epsilon}(\mathcal{S}_a)$ along the directions ∇F_j, $j = 1, 2$, are given by

$$d_j = \epsilon M_j + \mathcal{O}\big(\epsilon^2\big), \quad M_j = \int_{-\infty}^{+\infty} \langle \nabla F_j, f\rangle|_{u=U_H}\,\mathrm{d}t,$$

where $\langle , \rangle$ is the standard complex inner product. The integrand is evaluated along the homoclinic orbit of the plane wave solution $U_H(x,t)$, and ∇F_j is given by

$$\nabla F_j = -\mathrm{i}\frac{\sqrt{\Delta^2-4}}{W[\vec{\Psi}^{(+)}, \vec{\Psi}^{(-)}]} \begin{pmatrix} \Psi_2^{(+)}\Psi_2^{(-)} \\ \Psi_1^{(+)}\Psi_1^{(-)} \end{pmatrix}\Bigg|_{\lambda=\nu_j}, \tag{17}$$

with $\vec{\Psi}^{(+)}, \vec{\Psi}^{(-)}$ Bloch eigenfunctions at the new potential U_H evaluated at $\lambda = \nu_j$. The new Bloch basis can be obtained by means of a Bäcklund transformation; one also obtains the compact representation for the Wronskian $W[\vec{\Psi}^{(+)}, \vec{\Psi}^{(-)}] = (\lambda - \nu)(\lambda - \nu^*)W[\vec{\psi}^{(+)}, \vec{\psi}^{(-)}]$, which allows one to effortlessly evaluate the limit $\lambda \to \nu$ in Eq. (17).

In order to construct the Melnikov integrals, we first consider the limit $\lambda \to \nu_2$ and obtain

$$\nabla F_2 = C_2 \frac{W[\psi^{(+)}, \psi^{(-)}](\nu_2)}{(|\xi_1|^2 + |\xi_2|^2)^2} \begin{pmatrix} (\xi_1^*)^2 \\ (\xi_2^*)^2 \end{pmatrix}, \tag{18}$$

with

$$C_2 = \mathrm{i}d_+d_-(\nu_2 - \nu_2^*)(\nu_2 - \nu_1)(\nu_2 - \nu_1^*)\sqrt{\Delta(\nu_2)\Delta''(\nu_2)},$$

and with $\xi(\nu_2) = G(\nu_2, \nu_1; \phi(\nu_1))\chi(\nu_2)$. Here $G(\nu_2, \nu_1; \phi(\nu_1))$ is the gauge matrix which carries eigenfunctions $\phi(\lambda)$ of the plane wave solution to eigenfunctions $\xi(\lambda)$ of u_1, the potential obtained after one iteration of the Bäcklund formula, and $\chi(\nu_2) = d_+\psi^{(+)}(\nu_2) + d_-\psi^{(-)}(\nu_2)$. This leads to the following Melnikov integral

$$M_2(\gamma) = C_2 \int_{-\infty}^{+\infty}\int_0^1 W\big[\psi^{(+)}, \psi^{(-)}\big] \frac{(\xi_1^*)^2(U_H)_{xxxx} - (\xi_2^*)^2(U_H^*)_{xxxx}}{(|\xi_1|^2 + |\xi_2|^2)^2}\,\mathrm{d}x\,\mathrm{d}t. \tag{19}$$

Similarly, computing the limit $\lambda \to \nu_1$ leads to the following expression for ∇F_1:

$$\nabla F_1 = C_1 \frac{W[\psi^{(+)}, \psi^{(-)}](\nu_1)}{(|\zeta_1|^2 + |\zeta_2|^2)^2} \begin{pmatrix} (\zeta_1^*)^2 \\ (\zeta_2^*)^2 \end{pmatrix}, \tag{20}$$

with $C_1 = \mathrm{i}c_+c_-(\nu_1 - \nu_1^*)(\nu_1 - \nu_2)(\nu_1 - \nu_2^*)\sqrt{\Delta(\nu_1)\Delta''(\nu_1)}$, and with $\zeta(\nu_1) = G(\nu_1, \nu_2; \chi(\nu_2))$. The corresponding Melnikov integral is

$$M_1(\gamma) = C_1 \int_{-\infty}^{+\infty}\int_0^1 W\big[\psi^{(+)}, \psi^{(-)}\big] \frac{(\zeta_1^*)^2(U_H)_{xxxx} - (\zeta_1^*)^2(U_H^*)_{xxxx}}{(|\zeta_1|^2 + |\zeta_2|^2)^2}\,\mathrm{d}x\,\mathrm{d}t. \tag{21}$$

The numerical evaluation of the two Melnikov integrals, using expression (12) for the homoclinic orbit of the unstable plane wave solution, indicate that M_1 and M_2 are mutually proportional functions of the parameter γ [24]. The presence of a unique nondegenerate zero of $M_1 \sim M_2$ suggests (together with numerical evidence of irregular behavior) a single measurement is sufficient for establishing persistence of invariant hyperbolic sets.

The value $\gamma = \gamma_0$, at which a nondegenerate zero of M_1 occurs is $\mathcal{O}(\epsilon)$-close to the value of γ for which the homoclinic solution (12) achieves maximum amplitude. Fig. 3(b) shows an amplitude plot of the homoclinic orbit with $\gamma = \gamma_0$. Remarkably, this solution can be identified with the rogue wave observed intermittently (see e.g. Fig. 5(a)) throughout the numerical simulations. While a Melnikov analysis usually only indicates persistence of hyperbolic

structures (which are the source of irregular dynamics), for the even MD equation it also supports the thesis that chaotic dynamics leads to optimal phase modulation and increases the likelihood of rogue wave events.

We finally remark that, due to the imposed spatial symmetry, the imaginary parts of the gradients ∇F_j vanish identically, while for the full MD equation the presence of symmetry breaking terms in the perturbation makes the Melnikov integrals complex quantities. Recently, we studied a simple symmetry breaking perturbation of the NLS equation, for which the existence of nondegenerate zeros of the real part of the Melnikov integral provides the condition for the onset of chaotic dynamics, while the existence of nondegenerate zeros of the imaginary part provides the condition for spatially asymmetric chaotic wave forms [32]. The question we are currently addressing is whether the presence of symmetry breaking terms (e.g. the odd terms in the MD equation) significantly changes the conditions for the onset of homoclinic chaos and the likelihood of rogue wave formation.

6. Random oceanic sea states

6.1. JONSWAP initial data

In this section we examine the generation of extreme waves for typical random oceanic sea states characterized by the Joint North Sea Wave Project (JONSWAP) power spectrum. The surface elevation η is related to u, the solution of the NLS equation, by $\eta = \mathrm{Re}\{\mathrm{i}u\,\mathrm{e}^{\mathrm{i}(k_0x-w_0t)}\}/\sqrt{2}k_0$. Using the Hilbert transform of η and its associated analytical signal, the initial condition for u can be modeled as the random wave process

$$u(x,0) = \sum_{n=1}^{N} C_n \exp\bigl[\mathrm{i}(k_{n-1}x - \phi_n)\bigr], \tag{22}$$

where C_n is the amplitude of the nth component with wave number $k_n = (n-1)k$, $k = 2\pi/L$, and random phase ϕ_n, uniformly distributed on the interval $(0, 2\pi)$. The spectral amplitudes, $C_n = -\mathrm{i}\sqrt{2S_n/L}$, are obtained from the JONSWAP spectrum [14]

$$S(f) = \frac{\alpha}{f^5}\exp\left[-\frac{5}{4}\left(\frac{f_0}{f}\right)^4\right]\gamma^r, \quad r = \exp\left[-\frac{1}{2}\left(\frac{f-f_0}{\sigma_0 f_0}\right)^2\right]. \tag{23}$$

Here f_0 is the dominant frequency, determined by the wind speed at a specified height above the sea surface, $\sigma_0 = 0.07$ (0.9) for $f \leqslant f_0$ ($f > f_0$) and $f_n = n/L$ is the wave frequency. The parameter γ is the peak-shape parameter; as γ is increased, the spectrum becomes narrower about the dominant peak. For $\gamma > 1$ the wave spectra continues to evolve through nonlinear wave-wave interactions even for very long times and distances. It is in this sense that JONSWAP spectra describe developing sea states rather than a fully developed sea.

The scale parameter α is related to the amplitude and energy content of the wavefield. Based on an "Ursell number", the ratio of the nonlinear and dispersive terms of the NLS equation (1) in dimensional form, the NLS equation is considered to be applicable for $2 < \gamma < 8$ [35]. Typical values of alpha are $0.008 < \alpha < 0.02$. In an earlier study of rogue waves in random oceanic sea states it was found that they occur more often for large values of the Phillips parameter α and the enhancement coefficient γ [35]. Even so, it was observed that large values of α and γ do not guarantee the development of extreme waves.

We analyse a nonlinear spectral decomposition of the JONSWAP initial data which takes into account, in addition to α and γ, the phase information ϕ_n. This decomposition is based upon the inverse spectral theory of the NLS equation, a procedure for solving the initial value problem analogous to Fourier methods for linear problems. We find a correlation between the occurrence of rogue waves in both the NLS and MD equations and the proximity in spectral space to homoclinic data of the NLS equation [15].

6.2. JONSWAP data and the proximity to homoclinic solutions of the NLS

The NLS and MD equations are numerically integrated using a pseudo-spectral scheme with 256 Fourier modes in space and a fourth order Runge–Kutta discretization in time ($\Delta t = 10^{-3}$). The nonlinear mode content of the data is numerically computed using the direct spectral transform described above, i.e. the system of ODEs (4) is numerically solved to obtain the discriminant Δ. The zeros of $\Delta \pm 2$ are then determined with a root solver based on

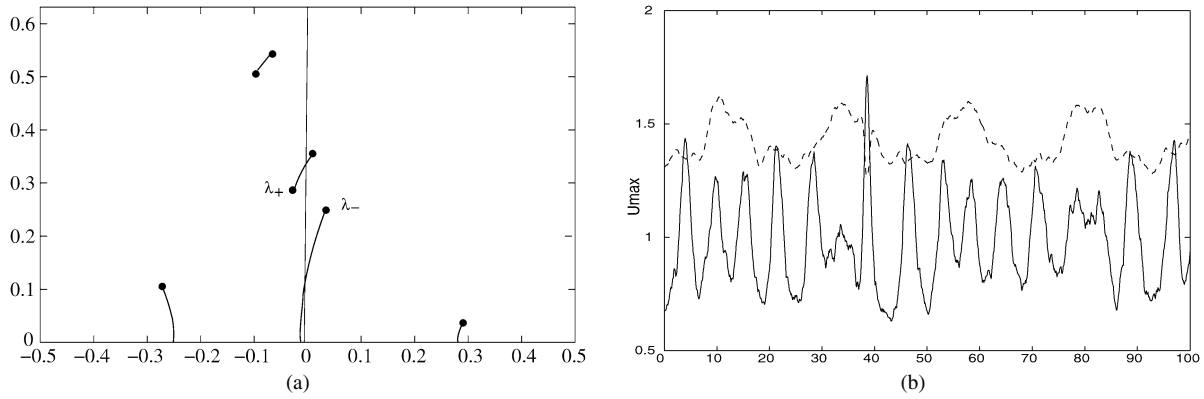

Fig. 8. (a) Nonlinear spectrum and (b) evolution of $U_{\max}$ for JONSWAP data ($\gamma = 4$ and $\alpha = 0.016$) that is near homoclinic data. Dashed curve corresponds to $2.2H_s$.

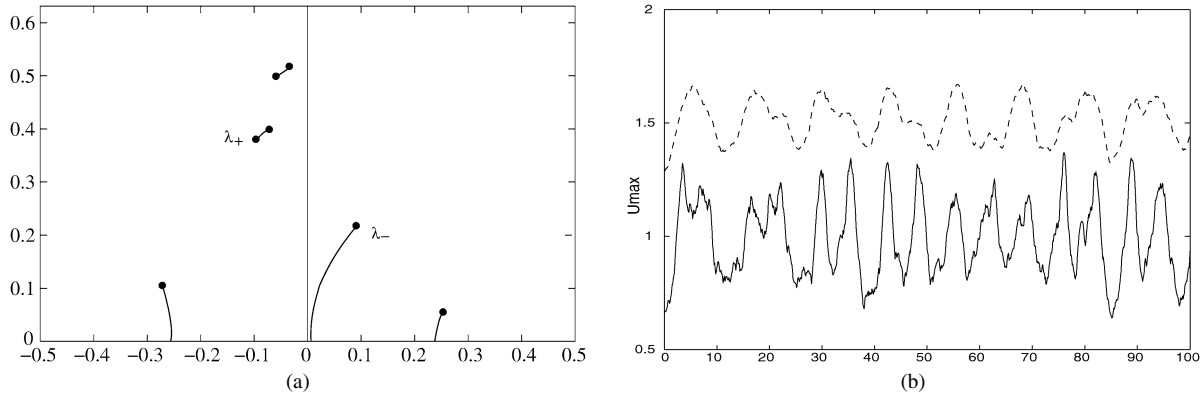

Fig. 9. (a) Nonlinear spectrum and (b) evolution of $U_{\max}$ for JONSWAP data ($\gamma = 4$ and $\alpha = 0.016$) that is far from homoclinic data. Dashed curve corresponds to $2.2H_s$.

Muller's method [17]. The spectrum is computed with an accuracy of $\mathcal{O}(10^{-6})$, whereas the spectral quantities we are interested in range from $\mathcal{O}(10^{-2})$ to $\mathcal{O}(10^{-1})$.

Complex double points typically split under perturbation into two simple points, $\lambda_{\pm}$, thus opening a gap in the band of spectrum (see Fig. 8(a)). We refer to the distance between these two simple points, $\delta(\lambda_+, \lambda_-) = |\lambda_+ - \lambda_-|$, as the splitting distance. Conversely, homoclinic solutions arise as an appropriate degeneration of a finite gap solution [36], i.e. for $\delta(\lambda_+, \lambda_-) \to 0$ and the resulting double point is complex. In this way we use δ to measure the proximity in the spectral plane to homoclinic data, i.e. to complex double points and their corresponding instabilities. Since the NLS spectrum is symmetric with respect to the real axis and real double points correspond to inactive modes, in subsequent plots only the spectrum in the upper half complex λ-plane will be displayed.

We begin by determining the spectrum of JONSWAP initial data given by (22) for various combinations of $\alpha = 0.008, 0.012, 0.016, 0.02$, and $\gamma = 1, 2, 4, 6, 8$. For each such pair (γ, α), we performed fifty simulations, each with a different set of randomly generated phases. As expected, the spectral configuration depends on the energy α and the enhancement coefficient γ. However, the extent of the dependence of features of the spectrum, such as the proximity to complex double points, upon the phases in the initial data was surprising.

Typical examples of the results are given in Figs. 8(a) and 9(a) which show the numerically computed nonlinear spectrum of JONSWAP initial data when $\gamma = 4$ and $\alpha = 0.016$ for two different realizations of the random phases. We find that JONSWAP data correspond to "semi-stable" N-phase solutions, i.e. we interpret the data as perturbations of N-phase solutions with one or more unstable modes (compare Fig. 8(a) with the spectrum of an unstable N-phase solution in Fig. 1). In Fig. 8(a) the splitting distance $\delta(\lambda_+, \lambda_-) \approx 0.07$, while in Fig. 9(a) $\delta(\lambda_+, \lambda_-) \approx 0.2$. Thus the JONSWAP data can be quite "near" homoclinic data as in Fig. 8(a) or "far" from homoclinic data as in Fig. 9(a), depending on the values of the phases ϕ_n in the initial data. For all the examined values of α and γ we find that, when

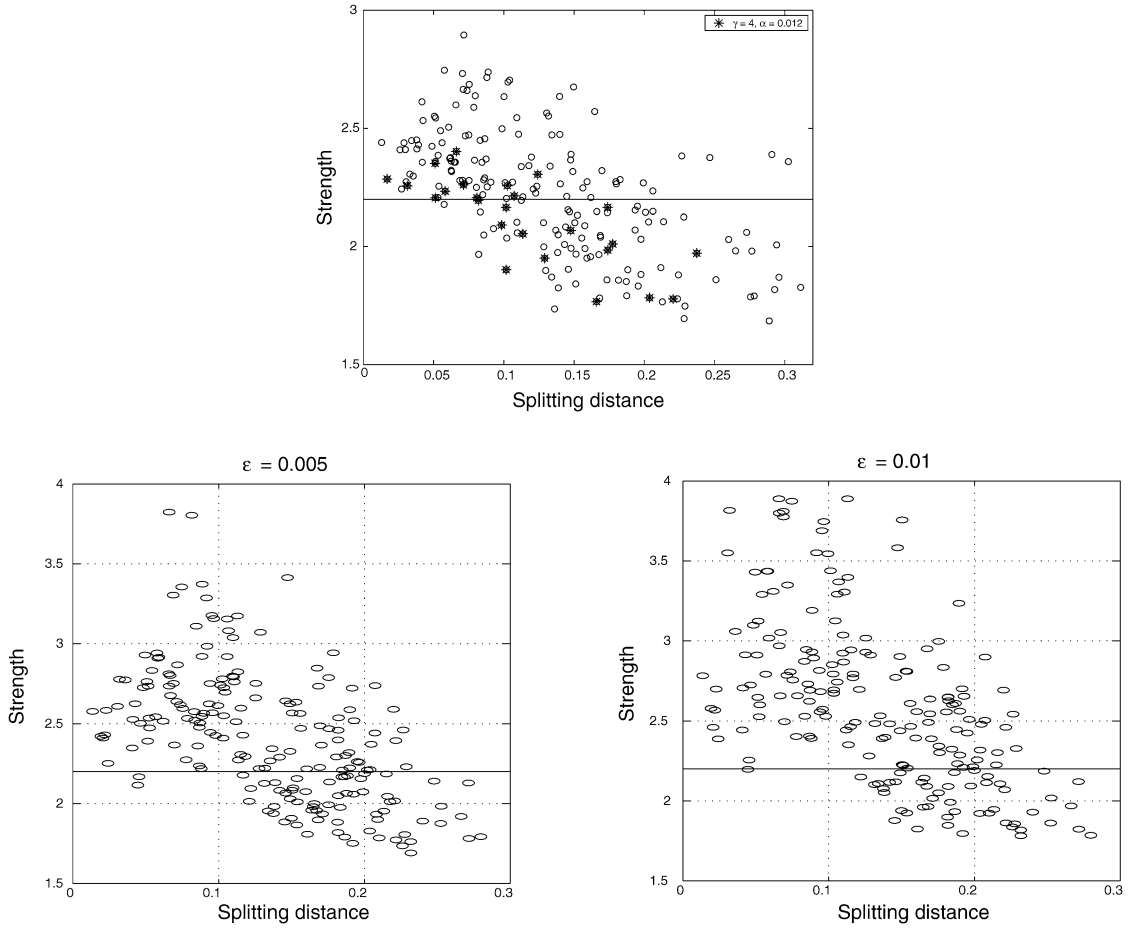

Fig. 10. Strength of $U_{\max}/H_s$ vs. the splitting distance $\delta(\lambda_+, \lambda_-)$.

α and γ are fixed, as the phases in the JONSWAP data vary, the spectral distance δ of typical JONSWAP data from homoclinic data varies.

Most importantly, irrespective of the values of the JONSWAP parameters α and γ, in simulations of the NLS equation (1) we find that extreme waves develop for JONSWAP initial data that is "near" NLS homoclinic data, whereas the JONSWAP data that is "far" from NLS homoclinic data typically does not generate extreme waves. Figs. 8(b) and 9(b) show the corresponding evolution of the maximum surface elevation, $U_{\max}$, obtained with the NLS equation. $U_{\max}$ is given by the solid curve and as a reference, $2.2H_S$ (the threshold for a rogue wave) is given by the dashed curve. H_S is the significant wave height and is calculated as four times the standard deviation of the wave amplitude. Fig. 8(b) shows that when the nonlinear spectrum is near homoclinic data, $U_{\max}$ exceeds $2.2H_S$ (a rogue wave develops at $t \approx 40$). Fig. 9(b) shows that when the nonlinear spectrum is far from homoclinic data, $U_{\max}$ is significantly below $2.2H_S$ and a rogue wave does not develop. As a result we can correlate the occurrence of rogue waves characterized by JONSWAP spectrum with the proximity to homoclinic solutions of the NLS equation.

The results of hundreds of simulations of the NLS and MD equations consistently show that proximity to homoclinic data is a crucial indicator of rogue wave events. Fig. 10 provides a synthesis of 200 random simulations of the NLS equation and of the MD equation for two perturbation strengths ($\epsilon = 0.005$ and $\epsilon = 0.01$) for JONSWAP initial data with different (γ, α) pairs (with $\gamma = 2, 4, 6, 8,$ and $\alpha = 0.012, 0.016$). For each such pair (γ, α), we performed 25 simulations, each with a different set of randomly generated phases. We restrict our consideration to semi-stable N-phase solutions near to unstable solutions of the NLS with one UM. Each circle represents the strength of the maximum wave ($U_{\max}/H_S$) attained during one simulation as a function of the splitting distance $\delta(\lambda_+, \lambda_-)$. The results for the particular pair ($\gamma = 4, \alpha = 0.012$) is represented with an asterisk. A horizontal line at $U_{\max}/H_S = 2.2$ indicates

the reference strength for rogue wave formation. We identify two critical values $\delta_1(\epsilon)$ and $\delta_2(\epsilon)$ that clearly show that (a) if $\delta < \delta_1$ (near homoclinic data) rogue waves will occur; (b) if $\delta_1 < \delta < \delta_2$, the likelihood of obtaining rogue waves decreases as δ increases and, (c) if $\delta > \delta_2$ the likelihood of a rogue wave occurring is extremely small.

This behavior is robust. As α and γ are varied, the strength of the maximum wave and the occurrence of rogue waves are well predicted by the proximity to homoclinic solutions. The individual plots of the strength vs. δ for particular pairs (γ, α) are qualitatively the same regardless of the pair chosen. As noted in Section 4 on the MD equation, enhanced focusing occurs in the chaotic regime. Fig. 10 shows that as ϵ increases the average strength and the likelihood of rogue waves increases. These results give strong evidence of the relevance of homoclinic solutions of the NLS equation in investigating rogue wave phenomena for more realistic oceanic conditions and identifies the nonlinear spectral decomposition as a simple diagnostic tool for predicting the occurrence and strength of rogue waves. Finally we remark that the nonlinear spectral analysis can be implemented for other types of general data in order to predict the occurrence of rogue waves.

7. Conclusions

In this paper we have investigated the modulational instability as a mechanism for the generation of rogue waves using simple model equations such as the NLS and MD equations. Using the integrable theory of the NLS, we obtained formulas for optimally phase modulated homoclinic orbits where the UMs are simultaneously excited leading to a significant amplification beyond the usual BF modulation instability.

The numerical results indicate that rogue waves are robust to the MD perturbation of the evolution equation. In fact, enhanced wave amplification is shown to occur in the chaotic regime. Significantly, we find that the wavefield is chaotic before the coalesced rogue waves appear, i.e. the chaos provides a mechanism for further focusing to occur due to chaotically generated optimal phase modulations.

The Melnikov analysis provides necessary conditions for the persistence of a homoclinic solution in the MD system which is $\mathcal{O}(\epsilon)$-close to the phase modulated or coalesced NLS homoclinic solution. The Melnikov analysis determines the distinguishing spatial features of the perturbed dynamics which agree with the numerical observations of high amplitude rogue waves in the MD chaotic regime. The correlation of the results of the Melnikov analysis to the MD numerical experiments indicates that in this more general setting homoclinic solutions of the NLS equation can be used to approximate rogue waves.

The machinery of inverse spectral theory for the NLS equation associates to each solution the spectrum of a certain linear operator. Introducing the "splitting distance" between simple points in the discrete spectrum of the AKNS system, we use it to determine the proximity in spectral space to instabilities of solutions of the NLS equation and their homoclinic orbits. The results of several hundred simulations of the NLS and MD equations, where the parameters and phases in the JONSWAP initial data are varied, indicate that rogue waves develop whenever the splitting distance is small, and do not occur when the splitting distance is large. In this way we correlate the development of rogue waves in oceanic sea states characterized by the JONSWAP spectrum with the proximity to homoclinic solutions of the NLS equation.

Acknowledgements

This work was partially supported by grant NSF-DMS0438154 of the National Science Foundation, U.S.A.

Appendix A. Statistical diagnostics

In the numerical experiments we monitor the evolution of the third and fourth statistical moments of the (probability density function of the wave amplitude) wavefield

$$M_3(a) = \sum_{j=1}^{N} \frac{(a_j - \bar{a})^3}{N}, \qquad M_4(a) = \sum_{j=1}^{N} \frac{(a_j - \bar{a})^4}{N},$$

where $\bar{a}$ is the mean height of the wavefield, and N is the number of data points sampled. The skewness, m_3, and the kurtosis, m_4, of the wavefield are then given by

$$m_3(a) = \frac{M_3}{\sigma^3}, \qquad m_4(a) = \frac{M_4}{\sigma^4},$$

where σ is the standard deviation.

Skewness is a measure of the vertical asymmetry of the wavefield. Positive values indicate the wavefield is skewed above average height, i.e. the crests are bigger than the troughs. Negative values indicate that the wavefield is skewed below average height.

The kurtosis is a measure of whether the distribution for the wavefield is peaked or flat, relative to a Gaussian distribution and defines the contribution of large waves to the wavefield. Wavefields with high kurtosis tend to have a distinct peak near the mean, decline rapidly, and have heavy tails. That is the larger the value of the kurtosis, the large/wider the tails of the pdf. The kurtosis for a Gaussian distribution is three. For this reason, excess kurtosis much above three indicates that the contribution of large waves is significant and corresponds to a higher probability of a rogue wave event.

References

[1] B.S. White, B. Fornberg, On the chance of freak waves at sea, J. Fluid Mech. 355 (1998) 113–138.
[2] C. Kharif, E. Pelinovsky, Physical mechanisms of the rogue wave phenomenon, Eur. J. Mech. B Fluids 22 (2004) 603–634.
[3] K.L. Henderson, D.H. Peregrine, J.W. Dold, Unsteady water wave modulations: fully nonlinear solutions and comparison with the nonlinear Schrödinger equation, Wave Motion 29 (1999) 341.
[4] K. Dysthe, K. Trulsen, Note on breather type solutions of the NLS as model for freak waves, Phys. Scripta 82 (1999) 48–52.
[5] M. Olagnon, G. Athanassoulis (Eds.), Rogue Waves 2000, Ifremer 32, 2001.
[6] V.E. Zakharov, A.B. Shabat, Exact theory of two-dimensional self-focusing and one-dimensional self-modulation of waves in nonlinear media, Sov. Phys. JETP 34 (1972) 62–69.
[7] M. Ablowitz, H. Segur, Solitons and the Inverse Scattering Transform, SIAM, 1981.
[8] K. Trulsen, K. Dysthe, A modified nonlinear Schrödinger equation for broader bandwidth gravity waves on deep water, Wave Motion 24 (1996) 281.
[9] K. Trulsen, K. Dysthe, Frequency downshift in three-dimensional wave trains in a deep basin, J. Fluid Mech. 352 (1997) 359–373.
[10] A. Osborne, M. Onorato, M. Serio, The nonlinear dynamics of rogue waves and holes in deep-water gravity wave trains, Phys. Lett. A 275 (2000) 386.
[11] N. Ercolani, M.G. Forest, D.W. McLaughlin, Geometry of the modulational instability. Part III: Homoclinic orbits for the periodic Sine–Gordon equation, Physica D 43 (1990) 349–384.
[12] A. Calini, C. Schober, Homoclinic chaos increases the likelihood of rogue waves, Phys. Lett. A 298 (2002) 335–349.
[13] C. Kharif, E. Pelinovsky, Focusing of nonlinear wave groups in deep water, JETP Lett. 73 (2001) 170–175.
[14] M.K. Ochi, Ocean Waves: The Stochastic Approach, Cambridge University Press, 1998.
[15] A. Islas, C. Schober, Predicting rogue waves in random oceanic sea states, Phys. Fluids 17 (2005) 031701-4.
[16] N.M. Ercolani, D.W. McLaughlin, Toward a topological classification of integrable PDE's, in: R. Devaney, H. Flaschka, W. Meyer, T. Ratiu (Eds.), MSRI Proc. Workshop on Symplectic Geometry, 1990.
[17] N. Ercolani, M.G. Forest, D. McLaughlin, Geometry of the modulational instability III. Homoclinic orbits, Physica D 43 (1990) 349.
[18] A.R. Its, V.P. Kotljarov, Explicit formulas for solutions of a nonlinear Schrödinger equation, Dokl. Akad. Nauk Ukrain. SSR Ser. A 1051 (1976) 965–968.
[19] I.M. Krichever, Methods of algebraic geometry in the theory of nonlinear equations, Russian Math. Surv. 32 (1977) 185–213.
[20] E.D. Belokolos, A.I. Bobenko, V.Z. Enol'skii, A.R. Its, V.B. Matveev, Algebro-Geometric Approach to Nonlinear Integrable Equations, Springer, Berlin, 1994.
[21] D.W. McLaughlin, C.M. Schober, Chaotic and homoclinic behavior for numerical discretizations of the nonlinear Schrödinger equation, Physica D 57 (1992) 447–465.
[22] V.B. Matveev, M.A. Salle, Darboux Transformations and Solitons, Springer-Verlag, 1991.
[23] N.N. Akhmediev, V.I. Korneev, N.V. Mitskevich, N-modulation signals in a single-mode optical waveguide under nonlinear conditions, Sov. Phys. JETP 67 (1988) 1.
[24] A. Calini, N.M. Ercolani, D.W. McLaughlin, C.M. Schober, Physica D 89 (1996) 227–260.
[25] M.J. Ablowitz, J. Hammack, D. Henderson, C.M. Schober, Modulated periodic Stokes waves in deep water, Phys. Rev. Lett. 84 (2000) 887–890.
[26] M. Ablowitz, J. Hammack, D. Henderson, C. Schober, Long time dynamics of the modulational instability of deep water waves, Physica D 152–153 (2001) 416–433.
[27] J. Guckenheimer, P.J. Holmes, Nonlinear Oscillations, Dynamical Systems, and Bifurcations of Vector Fields, Springer-Verlag, New York, 1983.
[28] G. Haller, S. Wiggins, Orbits homoclinic to resonances: the Hamiltonian case, Physica D 66 (1992) 298–346.

[29] D. Cai, D.W. McLaughlin, K.T.R. McLaughlin, The nonlinear Schrödinger equation as both a PDE and a dynamical system, Preprint, 1995.
[30] Y. Li, Homoclinic tubes in the nonlinear Schrödinger equation under Hamiltonian perturbations, Progr. Theoret. Phys. 101 (1999) 559–577.
[31] Y. Li, D.W. McLaughlin, J. Shatah, S. Wiggins, Persistent homoclinic orbits for a perturbed nonlinear Schrödinger equation, Comm. Pure Appl. Math. 49 (1996) 1175–1255.
[32] A. Calini, C.M. Schober, Chaotic dynamics for a symmetry breaking perturbation of the NLS equation, J. Math. Comput. Simul. 55 (2001) 351–364.
[33] C. Zeng, Comm. Pure Appl. Math. 53 (2000) 1222–1283.
[34] Y. Li, D.W. McLaughlin, Comm. Math. Phys. 612 (1994) 175–214.
[35] M. Onorato, A. Osborne, M. Serio, S. Bertone, Freak wave in random oceanic sea states, Phys. Rev. Lett. 86 (2001) 5831.
[36] A.R. Its, M.A. Salle, A.V. Rybin, Teor. Mat. Fiz. 74 (1) (1988) 29–45.